Inexpensive method for producing macroporous silicon particulates (MPSPs) with pyrolyzed polyacrylonitrile for lithium ion batteries

Madhuri Thakur[1], Steven L. Sinsabaugh[2], Mark J. Isaacson[3], Michael S. Wong[1,4] & Sibani Lisa Biswal[1]

[1]Department of Chemical and Biomolecular Engineering, Rice University, Houston, TX 77005 USA, [2]Lockheed Martin Space Systems, Palo Alto, CA USA, [3]Lockheed Martin MS2, Akron, OH USA, [4]Department of Chemistry, Rice University, Houston, 77005 TX USA.

One of the most exciting areas in lithium ion batteries is engineering structured silicon anodes. These new materials promise to lead the next generation of batteries with significantly higher reversible charge capacity than current technologies. One drawback of these materials is that their production involves costly processing steps, limiting their application in commercial lithium ion batteries. In this report we present an inexpensive method for synthesizing macroporous silicon particulates (MPSPs). After being mixed with polyacrylonitrile (PAN) and pyrolyzed, MPSPs can alloy with lithium, resulting in capacities of 1000 mAhg^{-1} for over 600+ cycles. These sponge-like MPSPs with pyrolyzed PAN (PPAN) can accommodate the large volume expansion associated with silicon lithiation. This performance combined with low cost processing yields a competitive anode material that will have an immediate and direct application in lithium ion batteries.

Lithium ion (Li-ion) batteries continue to draw attention because higher energy and power density storage devices are required for applications ranging from portable consumer electronics to electric vehicles[1]. Researchers continue to focus on the development of new materials with higher capacities and longer lifetimes for the major components of Li-ion batteries. Here, we focus on research that improves anode performance while remaining competitive in cost. Graphite, with a theoretical capacity of 372 mAhg^{-1}, is the current anode material commercially utilized for lithium ion batteries. Silicon has a specific capacity of 3579 mAhg^{-1} at room temperature[2,3], thereby improving lithium storage capacity by nearly a factor of ten by weight. However, lithiated silicon undergoes a large volume expansion (~300%), causing severe cracking of the silicon and eventually electrode failure. A variety of silicon structures and silicon-carbon based composites have been examined in order to reduce the lithiation-induced stress and suppress the structural destruction of silicon believed to be the main cause of the capacity loss during charge/discharge[4–11]. Examples of these efforts include the use of pure Si micro and nanoscale particles[6], Si dispersed in an active/inactive matrix[4], Si mixed with different binders[8–11], as well as the amorphous[12,13] and crystalline[14] Si thin films. Other nanostructured silicon structures include Si nanowires[15], Si core-shell nanowires[16], Si nanosprings[17] and Si-C nanocomposite granules[18], have demonstrated improved capacities and cycleability over bulk Si. However, it should be noted that most studies with nanostructured Si electrodes in Li-ion batteries have been limited to 100 or fewer charge/discharge cycles.

Recently, composite materials of porous silicon and carbon have also shown promising results. Bang et al.[19] have synthesized a macroporous silicon anode using silver (Ag) nanoparticles as a template to chemically etch silicon particles and coated them with a carbon layer using a thermal decomposition method. The material demonstrated a capacity of 2050 mAhg^{-1} for fifty cycles. Kim et al[20,21] have synthesized mesoporous Si/carbon core-shell nanowires as well as three dimensional (3-D) porous silicon(c-Si) particles. The pores in the Si-C composite provide the volume needed for the silicon expansion and allow fast transport of the lithium ions to the silicon and the carbon improves the stability of the solid electrolyte interface (SEI)[22], offers structural integrity and high electric conductivity[23]. Ge et al.[24] have also shown that silicon nanowires grown and then scraped off from a substrate can be combined with an alginate binder. They showed that this form of silicon,

with high porosity and large pore sizes, results in materials with capacities over 1000 mAhg^{-1} for hundreds of cycles.

Though the aforementioned materials promise much higher specific capacities and longer cycle life than commercial anode materials, they require a difficult and expensive processing step that oftentimes produces very limited quantities of material, limiting their potential for commercialization. We have previously developed a freestanding macroporous silicon films as an anode for lithium ion batteries[25]. These films offer a large surface area to volume ratio with controllable pore diameters. But these films cannot be conveniently incorporated into current battery processing techniques, which utilize material slurries and roll-to-roll processing. To design a more processable material, we changed from a film structure to a particulate structure that can be combined with PAN, or any binder, to form slurry that can be processed with standard coating technologies. Here we report an inexpensive wet etch processing technique that can be used to generate gram quantities of macroporous silicon particulates (MPSPs). When these are combined with polyacrylonitrile (PAN) and pyrolyzed, MPSPs can be cycled at a fixed capacity of 1000 mAhg^{-1} over 550 cycles.

Results

Macroporous silicon particulate (MPSP) characterization. A multistep lift-off process is used to fabricate freestanding macroporous silicon films that are on the order of 50–100 microns thick with pore diameters greater than 50 nm[25]. Our process allows us to control the thickness, pore diameter and the porosity by controlling the etching parameters such as current applied, wafer resistivity, concentration of electrolyte and doping of the wafer. After lift-off, the freestanding macroporous silicon film is ultrasonically fractured to create particulates with a nominal size range of 10–50 microns. The macroporous silicon particulates (MPSPs) are then mixed with

PAN to form a slurry, which is coated onto a current collector using a drop cast method and pyrolyzed to form an anode (see Materials and Methods for details). **Figure 1a** illustrates the preparation of the freestanding macroporous silicon films, the sonication to form MPSPs, and the combination of MPSPs with PAN and pyrolyzed. This wet-etch process does not require costly vacuum or deposition processing, making it less costly compared to other silicon structures. Because the underlying bulk silicon substrate can be reused to create another layer of macroporous silicon, there is little silicon waste in our process. Using the actual price of bulk silicon wafers used in our process as \$29/kg, MPSP with pyrolyzed PAN (PPAN) costs \$0.024 A^{-1}h^{-1}, which is competitive with existing graphitic carbon anodes, which is priced at \$0.013 A^{-1}h^{-1} [26]. Additionally, since these particulates are tens of microns, this material does not suffer from safety and health concerns associated with silicon nanoparticles[27].

Figure 1b shows scanning electron microscopic (SEM) images for the freestanding macroporous silicon film, MPSPs, MPSPs mixed with PAN, and the composite material after pyrolysis. Chemical characterization comparing the MPSPs with and without PPAN is performed using energy–dispersive X-Ray spectroscopy (EDX), X-Ray diffraction (XRD) and X-ray photoelectron spectroscopy (XPS). EDX and XRD of MPSPs with PPAN shows only a carbon and silicon signature, which indicates there is no formation of silicon carbide and negligible impurities in the material. Both techniques also exhibit identical silicon peaks for the materials. From XRD, the MPSPs with PPAN exhibit a weak and broad diffraction peak $2\theta = 25.96°$, characteristic of a disordered carbon structure (spectra shown in **Figure S1 and S2** in supplementary material)[28]. Wide scan XPS analysis reveals the composition of the exterior surface of the MPSPs/PPAN material. The XPS analysis shows major peaks that are due to carbon (C1s), oxygen (O1s), nitrogen (N1s) and silicon (Si2s and Si2p). High resolution scans for the elements of carbon (C 1s)
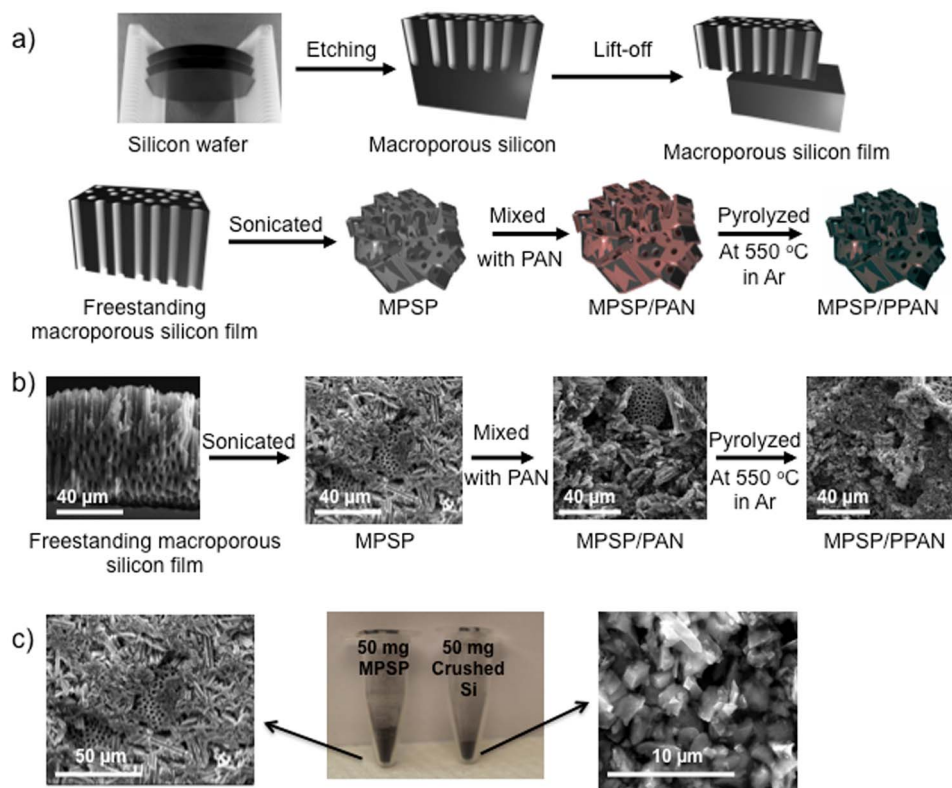

Figure 1 | (a) Description of process to generate a MPSP/PPAN composite material from a free standing macroporous silicon film. (b) Corresponding scanning electron microscope (SEM) images for freestanding macroporous silicon film, a sonicated film forming macroporous silicon micro-particulates (MPSPs), MPSPs mixed with PAN, and MPSP/PPAN after pyrolysis; (c) SEM image and volume comparison between a 50mg powder sample of macroporous silicon micro-particulates (MPSP) and with crushed silicon particulates.

and nitrogen (N 1s) shows the appearance of C-N (286.14 eV)[29] and C-C, C-H and C=C(284.51)[30,31] in the C1s peak and and N≡C(398.1eV)[32], N=C(399.24 eV) and N-C(399.99 eV)[33] in the N 1s peak respectively (spectra shown in **Figure S3** in supplementary material). Our results are supported by the previous studies that suggest that PAN undergoes a structural transition to form a conjugated-chain structure that is able to act as both a binder and a conductive matrix for silicon[34–36].

From **Figure 1b**, it is noticeable that the MPSPs are disordered fragments of the macroporous silicon film. What is quite striking is that for the same mass of silicon, crushed silicon (formed by sonicating an untreated silicon wafer) has a much smaller volume compared to our macroporous silicon particulates, as shown in **Figure 1c**. The specific surface area of macroporous versus crushed silicon microparticulates, shown are measured via nitrogen adsorption using the Brunauer-Emmett-Teller (BET) method (isotherm shown in **Figure S4** in supplementary material). The BET surface area of MPSPs is 46.85 m^2 (STP)g^{-1}($\pm$ 0.12), whereas the crushed silicon micro-particulates have a surface area of 0.71 m^2(STP)g^{-1} ($\pm$0.08 m^2/g). Thus though the physical dimensions of two particulates are similar, the surface area of the MPSP is 40 times larger, indicating a highly porous silicon structure.

Electrochemical testing of MPSP. The electrochemical characteristics of the MPSPs/PPAN composite were examined using galvanostatic cycling at room temperature using a half-cell. A 2-electrode test cell (Hosen) was constructed using the MPSPs/PPAN composite as the anode, lithium foil as a counter electrode and a polymer as a separator (details described in Materials and Methods). **Figure 2a** compares the electrochemical performance of an anode comprised of MPSPs with PPAN versus untreated crushed silicon particulates from silicon wafer. Both samples had a nominal particulate size of order of 10-50 microns and a mass ratio of 7:3 for silicon to PAN. For the first two cycles the MPSPs/PPAN and non-porous silicon microparticles (NPSPs) with PPAN were charged and discharged at 200 μAcm^{-2} between 0.07 V and 1.0 V. From the third cycle onward, the cell was charged and discharged between 0-1V at a constant charge capacity of 1200mAhg^{-1}. The MPSP electrodes show good cycling stability with an average discharge capacity retention of 99% after 150 cycles, as shown by the blue lines in **Figure 2a**, whereas the crushed silicon electrode lost 75% or its discharge capacity in five cycles as shown by the brown lines in **Figure 2a**. Cui et al.[37] have also shown the silicon microparticles (8 μm and 15 μm diameters) with carbonized PAN and a uniform coating of a-Si by CVD have poor cycleability. The anode with MPSP/PPAN composite has a high capacity and longer cycle life as compared to the crushed silicon particulates. We believe that the better performance of the macroporous material in comparison to the non-porous materials is due to the greater porosity of the MPSP particulates, which can better accommodate the volume expansion of the silicon when alloying with lithium. Visual inspection of the crushed and MPSPs after 50 cycles (SEM images shown in **Figure S5** in supplementary material) show that the crushed silicon has large observable cracks while the MPSP maintains a porous structure.
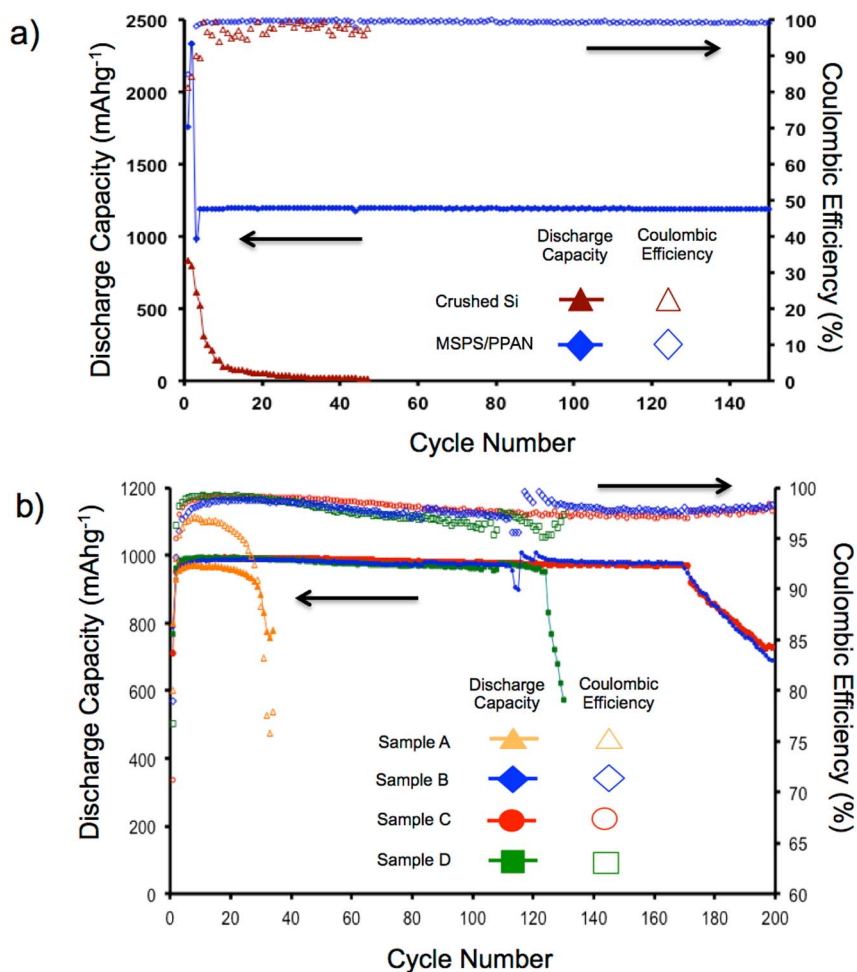

Figure 2 | (a) Comparison of the discharge capacity and coulombic efficiency of composite of MPSP versus crushed silicon particulates mixed with PPAN versus cycle number; (b) Comparison of the discharge capacity and coulombic efficiency of MPSPs/PPAN anodes at various ratios versus cycle number.

Table 1 | Various mass ratios of MPSP: PAN with their corresponding theoretical capacities tested for performance

Sample	Ratio of MPSP:PAN	Theoretical capacity of MPSP (mAhg^{-1})	Cycles at discharge capacity of 1000 mAhg^{-1}
A	9:1	3221	30
B	4:1	2863	170
C	7:3	2504	170
D	3:2	2147	123

To determine the optimum ratio of MPSPs with PPAN, various ratios of the composite were tested, as shown in **Table 1**. The mass per unit area of all samples tested is 2 mgcm^{-2}. To maximize the cycle life, all samples are charged/discharged at a constant charge capacity of 1000 mAhg^{-1} between 0-1V. The charge capacity in the electrochemical tests is fixed at 1000 mAh/g because Obrovac et al.[38] suggested that the volume expansion of the silicon can be limited by controlling the amount of lithium that intercalates into the silicon. This can greatly improve the number of useful cycles of the cell. Cui et al. also found that limiting the intercalation of the silicon between 30–50% of the maximum specific capacity resulted in extended cycle life and that charging silicon microparticles and nanoparticles at constant charge capacity increase the cycle life of the anode[37]. The electrochemical tests for all the samples are carried out at a charge/discharge rate of C/5. The cycle performance of the sample A, B C and D is compared in **Figure 2b**. Sample B and C provided better cycle life performances at constant charge capacity of 1000 mAh/g before discharge capacity fade as compared to sample A and D.

To further increase the cycle life of the material we tested the optimized sample C (mass ratio for MPSPs to PAN is 7:3) with an
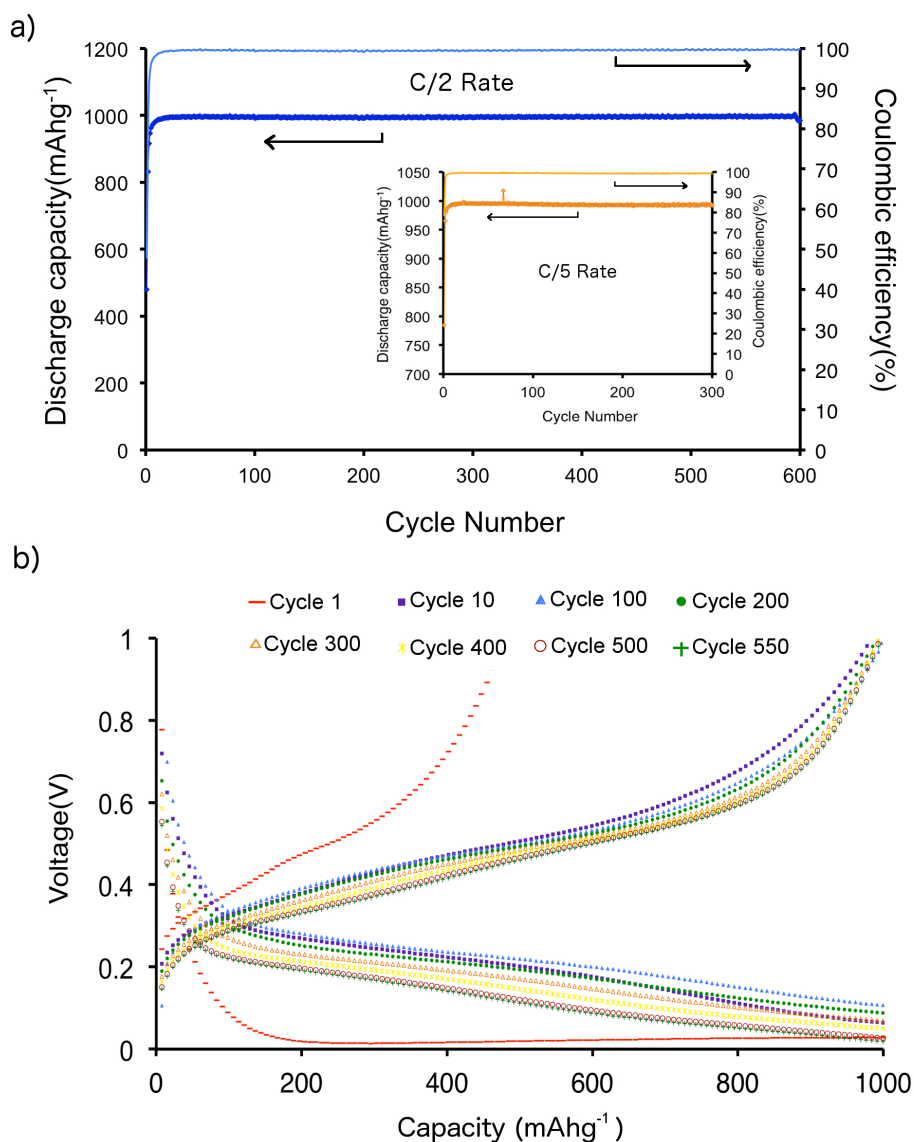

Figure 3 | (a) Discharge capacity and coulombic efficiency vs. cycle number for sample C (7:3) MPSPs/PPAN composite electrode using a fluorinated (FEC) electrolyte during galvanostatic charge/discharge between 0–1V at constant charge capacity of 1000 mAhg^{-1} for rate of C/2. Insert shows cycling between 0-1V at constant charge capacity of 1000 mAhg^{-1} for a rate of C/5. (b) Voltage profiles for sample C (7:3) MPSP/PPAN composite electrode with FEC after 1, 10, 100, 200, 300, 400, 500 and 550 cycles at a rate of C/2 between 0-1 V in half-cells at constant charge capacity of 1000 mAhg^{-1}.

electrolyte containing fluorinated ethylene carbonate electrolyte (FEC)[39]. The mass per unit area of the tested electrode is 2 mg cm^{-2} and has a theoretical specific capacity of 2505 mAhg^{-1}. Sample C is charged and discharged at a constant charge capacity of 1000 mAhg^{-1} at rate of C/5 and C/2 between 0-1V by using the fluorinated electrolyte. **Figure 3a** shows the discharge capacity and coulombic efficiency of MPSPs/PPAN composite versus cycle number at cycle rates of C/2. The capacity and coulombic efficiency of MPSPs/PPAN composite versus cycle number at cycle rates of C/5 is provided in the insert of **Figure 3a**. Also note that the coulombic efficiency for the first cycle is low (50% at C/2 and 82% at C/5). From the third cycle and onward, the coulombic efficiency is more than 99% and remains relatively stable over 600 cycles at C/2 and 300 cycles at C/5. The first cycle loss in the coulombic efficiency is related to the solid electrolyte interface (SEI) formation. The voltage profile in **Figure 3b** shows that the lithiation voltage for the fluorinated electrolyte decreases slowly, even after 500 cycles.

Discussion

Comparing the electrochemical testing results of the various ratios of MPSPs/PPAN, shown in Figure 2b, indicates that there is an optimum ratio. This is not surprising since Wang et. al. have shown that PPAN acts as a binder as well as a conducting material[40]. The cycle performance of Sample A indicates that there is insufficient PAN to provide structural support for the MPSPs, as well as a lack of conductive material, causing the sample to fail after 30 cycles. Samples D has more PAN relative to MPSP. It is able to run for more than 100 cycles, but the discharge capacity begins dropping after 120th cycles due to fact that the anode is cycling at a large percentage (47%) of its theoretical capacity, resulting in faster anode degradation. Sample B and C have the optimum ratio of MPSP and PAN. Both the samples are able to run for more then 200 cycles with a 30% fade in the total charge capacity after 170 cycles.

Interestingly, for Samples A-D, the full voltage range is not utilized initially. In particular for Sample C, the lower cut–off voltage continues to increase each cycle for the first 10 cycles. After 10 cycles, the material reaches a charge capacity of 1000 mAhg^{-1} close to 100 mV at C/5, as shown by the voltage profile in **Figure 4a**. The material is charged and discharged between these limits for 170 cycles. Once the cell reaches its lower cut-off voltage (0V) at 170 cycles for the sample using the non-fluorinated electrolyte and 596th cycles when using the fluorinated (FEC) electrolyte, the capacity begins fading. This indicates that material degradation occurs once the lower cut-off voltage is reached. Note that the capacity drop for Sample C with FEC (**Figure 3a**) is much slower as compared to the non-fluorinated electrolyte (**Figure 2b**). Comparison of the voltage profiles between the fluorinated and non-fluorinated electrolytes, **Figure 3b and Figure 4a** respectively, shows that the MPSPs/PPAN composite with FEC has a much slower change in the charge voltage range as compared to non-fluorinated electrolyte. The fluorinated electrolyte most likely forms a more stable solid electrolyte interface (SEI) layer, suppresses the electrolyte decomposition, and decreases battery resistance while increasing the specific capacity and cyclic stability[41].

Additionally for sample C, as shown in **Figure 4b**, the differential capacity curve for the 1st cycle during lithiation (Li insertion) shows only one broad peak from 0.23 to 0.08V, which is due to the phase transition of crystalline silicon to amorphous Li$_{15}$Si$_4$[3,41]. During delithiation (Li extraction) the differential capacity peaks at 0.3V and 0.47V are due to the phase transition between different amorphous Li$_x$Si phases[3]. The lithiation for the second cycle shows extra peaks at 0.24V, which corresponds to a higher voltage lithiation of amorphous Si-Li phase[38]. Kim et al.[20] have reported other peaks at 0.05V, which are not present in our system, which can be attributed to their material lithiating at a lower cut off voltage ($<$ 70 mV), whereas MPSPs/PPAN is lithiating at a lower cut off voltage greater than 100 mV for its initial 100 cycles at constant charge capacity. The
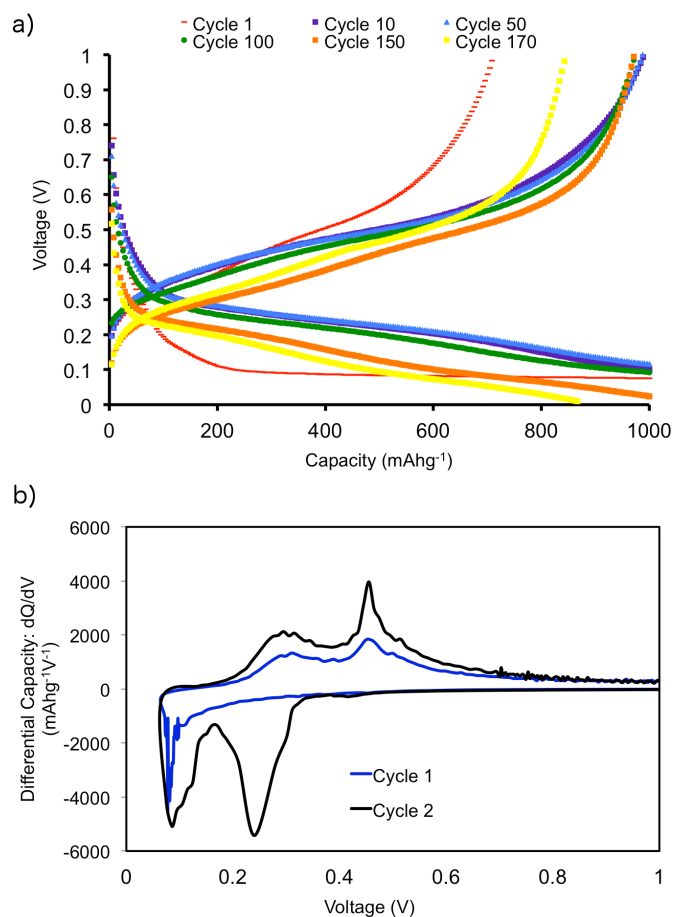

Figure 4 | (a) Voltage profiles for Sample C (7:3) MPSP/PPAN composite electrode using a non-fluorinated electrolyte after 1, 10, 50, 100, 150 and 170 cycles at a rate of C/5 between 0-1 V in half-cells at constant charge capacity of 1000 mAhg^{-1}. (b) Differential capacity curve for Sample C (7:3) MPSP/PPAN composite electrode in a non-fluorinated electrolyte after 1st and 2nd cycle.

increase in the delithiation peaks height after the first cycle indicates improvement in lithium extraction kinetics.

In summary, these results show that an anode comprised of MPSPs with PPAN significantly improves the cycle life compared to that of an anode fabricated from silicon particulates that do not contain pores. The PPAN functions as both a binder and conductive additive. The improved performance is attributed to the porosity of the MPSPs, which is able to accommodate the volume expansion associated with the lithiation of silicon. With use of the FEC electrolyte, cycleability increases by more than 600 cycles. The specific capacity and cycle life is comparable or oftentimes better than reported silicon micro and nanostructures. Combined with the low cost processing for large quantities of active material, MPSPs have the potential to transform the energy storage landscape. In the future, the cycleability of macroporous silicon micro-particulates will be further optimized by changing the electrochemical testing conditions, sonication time, pore size and binding material.

Methods

MPSP preparation. As described previously, a freestanding macroporous silicon film is synthesized by electrochemical etching of prime grade, boron doped, p-type (100) silicon wafers (Siltronix Corp.), of 275 μm thickness and resistivity's between 14-22 Ω-cm, in 48% hydrofluoric acid (HF, Sigma Aldrich) and dimethylformamide (DMF, Sigma Aldrich) at a constant current density of 2 mAcm^{-2} at room temperature[25]. The resulting freestanding porous silicon is lifted from the bulk silicon by applying a current density of 20 mAcm^{-2}. The freestanding hydrogen-terminated porous silicon film was then rinsed with methanol and DI water to remove any residue. MPSPs are

synthesized by sonicating (Branson 1210R-dth, 80W, 47KHz) 1g of free-standing macroporous silicon in 10 ml of dimethylformamide (DMF, Sigma Aldrich). A solution of 1g of polyacrylonitrile (PAN, Sigma Aldrich) was dissolved into 10 ml of DMF over 4 hours with stirring at 60°C. Then the PAN solution is mixed with the previously prepared macroporous silicon particulates at ratios of 3:2, 7:3, 4:1 and 9:1, by stirring at the same temperature for 6 hours. The slurry is coated onto the 25 μm thick stainless steel foil (Type, 304 Alfa Aesar) and heated for one hour at 550°C under an argon atmospheres.

Characterization. The weight % of the macroporous silicon micro-particulates and PAN was estimated by using the high-precision analytic balance (AND HR-202i, A&D company). The mass of the active materials was estimated by same analytic balance after pyrolyzing the PAN. SEM and EDAX observations were carried out by using a Quanta 400 ESEM (FEI) that has a resolution of 1.2nm at 30Kv and is equipped with an EDX detector. The XRD studies were carried out using a Rigaku D/Max Ultima II Powder equipped with an incident monochromator and vertical theta/theta goniometer. The system use only the Kα1 component of Cu radiation, improving the overall quality of the collected powder diffraction data. An accelerating voltage of 40Kv, current of 40 mA and 2θ-step of 0.02 were selected. The XRD data analysis was performed by JADE software (Materials Data Inc.). The surface analysis was done using a PHI Quantera Scanning X-Ray Microprobe. The pass energy was 26.0 eV for elemental scans and 140.0 eV for survey scans. The X-ray source was monochromatic Al Kα (1486.7 eV) and beam size was 200 um. The nitrogen adsorption and desorption isotherm were collected at 77K in a range of relative pressure of 0.0001-0.99P/P$_o$ using ASAP 2012 surface area measurement system from (Micromeritics). After drying the 250mg of sample under vacuum for 24 hours it was degassed under N$_2$ gas flow at 250°C for 12 hours before weighting and gas sorption measurements. The relative pressure range P/P$_o$ from 0.01 to 0.08 was used for multipoint Brunauer-Emmett-Teller (BET) calculations.

Electrochemical testing. A three and two electrode electrochemical cell (Hosen Test cell, Hohsen Corp. Japan) was used for all electrochemical measurements. Working electrode was prepared by drop casting the slurry of composite of macroporous silicon micro-particulates/PAN on stainless steel and pyrolyzed at 550 degree centigrade at Ar atmosphere. Lithium foil (0.75 mm thick, Alfa Aesar) was used as a counter electrode. A trilayer polypropylene membrane (Celgard 2325) wetted with an electrolyte is used as a separator. The electrolyte used was 1 M LiPF$_6$ in a 1:1 ratio w/w ethylene carbonate: diethyl carbonate (Ferro Corporation) or a 1:1 ratio w/w FEC(Ferro Corporation): dimethyl carbonate (Sigma Aldrich). The anode material is not exposed to air before assembling into the cell. All the cells were assembled in an argon-filled glove box (<5ppm of oxygen and water, Vacuum Atmospheres Co.). The electrochemical testing is performed using Arbin Instruments' BT2000. Our anode material is charged/discharged between 0 and 1V versus Li/Li+ at C/5 and C/2 for constant charge capacity (CCC). The coulombic efficiency was calculated as 100%* (delithiation capacity/lithiation capacity).

1. Besenhard, J. O., Yang, J. & Winter, M. Will advanced lithium-alloy anodes have a chance in lithium-ion batteries? *J. Power Sources* **68**, 87–90 (1997).
2. Obrovac, M. N., Christensen, L., Le, D. B. & Dahnb, J. R. Alloy design for lithium-ion battery anodes. *J. Electrochem. Soc.* **154**, A849–A855 (2007).
3. Li, J. & Dahn, J. R. An in situ X-ray diffraction study of the reaction of Li with crystalline Si. *J. Electrochem. Soc.* **154**, A156–A161 (2007).
4. Kim, I., Kumta, P. N. & Blomgren, G. E. Si/TiN nanocomposites - Novel anode materials for Li-ion batteries. *Electrochem. Solid State Lett.* **3**, 493–496 (2000).
5. Kim, J. W., Ryu, J. H., Lee, K. T. & Oh, S. M. Improvement of silicon powder negative electrodes by copper electroless deposition for lithium secondary batteries. *J. Power Sources* **147**, 227–233 (2005).
6. Kasavajjula, U., Wang, C. S. & Appleby, A. J. Nano- and bulk-silicon-based insertion anodes for lithium-ion secondary cells. *J. Power Sources* **163**, 1003–1039 (2007).
7. Tarascon, J. M. & Armand, M. Issues and challenges facing rechargeable lithium batteries. *Nature* **414**, 359–367 (2001).
8. Ng, S. B., Lee, J. Y. & Liu, Z. L. Si-O network encapsulated graphite-silicon mixtures as negative electrodes for lithium-ion batteries. *J. Power Sources* **94**, 63–67 (2001).
9. Weydanz, W. J., Wohlfahrt-Mehrens, M. & Huggins, R. A. A room temperature study of the binary lithium-silicon and the ternary lithium-chromium-silicon system for use in rechargeable lithium batteries. *J. Power Sources* **81**, 237–242 (1999).
10. Li, H., Huang, X. J., Chen, L. Q., Wu, Z. G. & Liang, Y. A high capacity nano-Si composite anode material for lithium rechargeable batteries. *Electrochem. Solid State Lett.* **2**, 547–549 (1999).
11. Li, J., Christensen, L., Obrovac, M. N., Hewitt, K. C. & Dahn, J. R. Effect of heat treatment on Si electrodes using polyvinylidene fluoride binder. *J. Electrochem. Soc.* **155**, A234–A238 (2008).
12. Yang, H. et al. Amorphous Si film anode coupled with LiCoO2 cathode in Li-ion cell. *J. Power Sources* **174**, 533–537 (2007).
13. Maranchi, J. P., Hepp, A. F., Evans, A. G., Nuhfer, N. T. & Kumta, P. N. Interfacial properties of the a-Si/Cu : active-inactive thin-film anode system for lithium-ion batteries. *J. Electrochem. Soc.* **153**, A1246–A1253 (2006).
14. Beaulieu, L. Y., Eberman, K. W., Turner, R. L., Krause, L. J. & Dahn, J. R. Colossal reversible volume changes in lithium alloys. *Electrochem. Solid State Lett.* **4**, A137–A140 (2001).
15. Chan, C. K. et al. High-performance lithium battery anodes using silicon nanowires. *Nature Nanotechnol.* **3**, 31–35 (2008).
16. Cui, L. F., Ruffo, R., Chan, C. K., Peng, H. L. & Cui, Y. Crystalline-Amorphous Core-Shell Silicon Nanowires for High Capacity and High Current Battery Electrodes. *Nano Lett.* **9**, 491–495 (2009).
17. Teki, R. et al. Nanostructured Silicon Anodes for Lithium Ion Rechargeable Batteries. *Small* **5**, 2236–2242 (2009).
18. Magasinski, A. et al. High-performance lithium-ion anodes using a hierarchical bottom-up approach. *Nature Mater.* **9**, 353–358 (2010).
19. Bang, B. M. et al. High-Performance Macroporous Bulk Silicon Anodes Synthesized by Template-Free Chemical Etching. *Adv. En. Mater.* **2**, 878–883 (2012).
20. Kim, H. & Cho, J. Superior Lithium Electroactive Mesoporous Si@Carbon Core-Shell Nanowires for Lithium Battery Anode Material. *Nano Lett.* **8**, 3688–3691 (2008).
21. Kim, H., Han, B., Choo, J. & Cho, J. Three-Dimensional Porous Silicon Particles for Use in High-Performance Lithium Secondary Batteries. *Angew. Chem. Int. Ed.* **47**, 10151–10154 (2008).
22. Yen, Y.-C., Chao, S.-C., Wu, H.-C. & Wu, N.-L. Study on Solid-Electrolyte-Interphase of Si and C-Coated Si Electrodes in Lithium Cells. *J. Electrochem. Soc.* **156**, A95–A102 (2009).
23. Baughman, R. H., Zakhidov, A. A. & de Heer, W. A. Carbon nanotubes - the route toward applications. *Science* **297**, 787–792 (2002).
24. Ge, M., Rong, J., Fang, X. & Zhou, C. Porous Doped Silicon Nanowires for Lithium Ion Battery Anode with Long Cycle Life. *Nano Lett.* **12**, 2318–2323 (2012).
25. Thakur, M. et al. Freestanding macroporous silicon and pyrolyzed polyacrylonitrile composite as an anode for lithium ion batteries. *Chem. Mater* **24**, 2998–3003 (2012).
26. Broddarp, R. J. Li-Ion Battery/Cell Manufacturing Cost Comparisons. *The 15th International Meeting on Lithium Ion Batteries - IMLB 2010 Montreal, Canada* (2010).
27. Napierska, D., Thomassen, L. C. J., Lison, D., Martens, J. A. & Hoet, P. H. The nanosilica hazard: another variable entity. *Particle and Fibre Toxicology* **7**, (2010).
28. Sandi, G., Winans, R. E. & Carrado, K. A. New carbon electrodes for secondary lithium batteries. *J. Electrochem. Soc.* **143**, L95–L98 (1996).
29. Labjar, N. et al. Enhanced corrosion resistance properties of carbon steel in hydrochloric acid medium by aminotris-(methylenephosphonic): Surface characterizations. *J. Mater. Environ. Sci.* **2** 309–318 (2011).
30. Wielant, J., Hauffman, T., Blajiev, O., Hausbrand, R. & Terryn, H. Influence of the iron oxide acid-base properties on the chemisorption of model epoxy compounds studied by XPS. *J. Phys. Chem. C* **111**, 13177–13184 (2007).
31. Okpalugo, T. I. T., Papakonstantinou, P., Murphy, H., McLaughlin, J. & Brown, N. M. D. High resolution XPS characterization of chemical functionalised MWCNTs and SWCNTs. *Carbon* **43**, 153–161 (2005).
32. Zheng, W. T. et al. N1s electron binding energies of CNx thin films grown by magnetron sputtering at different temperature. *J. Mater. Sci.Technol.* **14**, 25–28 (1998).
33. Chang, C. F., Chen, W. C., Wen, T. C. & Gopalan, A. Electrochemical and spectroelectrochemical studies on copolymerization of diphenylamine with 2,5-diaminobenzenesulfonic acid. *J. Electrochem. Soc.* **149**, E298–E305 (2002).
34. Xue, J. S. & Dahn, J. R. DRAMATIC EFFECT OF OXIDATION ON LITHIUM INSERTION IN CARBONS MADE FROM EPOXY-RESINS. *J. Electrochem. Soc.* **142**, 3668–3677 (1995).
35. Kim, C., Yang, K. S., Kim, Y. J. & Endo, M. Heat treatment temperature effects on structural and electrochemical properties of PVDC-based disordered carbons. *J. Mater. Sci.* **38**, 2987–2991 (2003).
36. Janus, R. et al. Thermal transformation of polyacrylonitrile deposited on SBA-15type silica. *J Therm. Anal. Calorim.* 1–7 (2012).
37. Cui, L.-F., Hu, L., Wu, H., Choi, J. W. & Cui, Y. Inorganic Glue Enabling High Performance of Silicon Particles as Lithium Ion Battery Anode. *J. Electrochem. Soc.* **158**, A592–A596 (2011).
38. Obrovac, M. N. & Krause, L. J. Reversible cycling of crystalline silicon powder. *J. Electrochem. Soc.* **154**, A103–A108 (2007).
39. Nakai, H., Kubota, T., Kita, A. & Kawashima, A. Investigation of the Solid Electrolyte Interphase Formed by Fluoroethylene Carbonate on Si Electrodes. *J. Electrochem. Soc.* **158**, A798–A801 (2011).
40. Wang, L., Yu, Y., Chen, P. C., Zhang, D. W. & Chen, C. H. Electrospinning synthesis of C/Fe3O4 composite nanofibers and their application for high performance lithium-ion batteries. *J. Power Sources* **183**, 717–723 (2008).
41. Kang, Y.-M. et al. Phase transitions explanatory of the electrochemical degradation mechanism of Si based materials. *Electrochem. Commun.* **9**, 959–964 (2007).

Author contributions

M.T. and S.L.B. designed and performed the research; M.J.I contributed new experimental reagents; data was interpreted by M.T., M.J.I, S.L.S. and S.L.B. M.T. wrote the manuscript with support from M.J.I., S.L.S., M.S.W. and S.L.B.

Additional information

Supplementary information accompanies this paper at http://www.nature.com/scientificreports